



Thermal evolution of gels prepared by chelation of aluminum sec-butoxide with ethyl acetoacetate in various amounts

S. Kurajica¹ · K. Mužina¹ · I. Simčić² · V. Mandić¹

Received: 1 September 2021 / Accepted: 9 June 2022 / Published online: 1 July 2022
© Akadémiai Kiadó, Budapest, Hungary 2022

Abstract

This work presents a thermal evolution study of gels obtained by chelation of aluminum sec-butoxide (Asb) with ethyl acetoacetate (Eaa) in various amounts. Samples were characterized by scanning electron microscopy (SEM), low angle laser light scattering (LALLS), differential thermal and thermo-gravimetric analysis (DTA/TGA), Fourier-transformed infra-red spectroscopy (FTIR) and X-ray diffraction (XRD). It was established that samples with a low Eaa/Asb ratio are mainly amorphous, whilst the samples with greater Eaa/Asb ratio are predominantly chelate. The crystallization of γ -Al₂O₃ takes place between 600 and 1000 °C in two separate processes for all investigated samples. On the other hand, a complete transition to α -Al₂O₃ at 1200 °C occurs exclusively in samples with high Eaa/Asb ratio, while it is only partial for samples with low Eaa/Asb ratio. The observed mass loss is in concordance with the hypothesis that the overall gel content in the samples could be represented by a simplified formula Al(Eaa)_xO_{(3-x)/2}, where x is the Eaa/Asb ratio. In addition to thermal evolution, the gel-chelate duality of the samples is reflected in the morphology and particle size distribution.

Keywords Alumina · Sol–gel · Chelation · Thermal analysis

Introduction

Alumina, Al₂O₃, can exist as a stable polymorph (α) or as one of the metastable phases (γ , θ , η , χ , δ , and κ), commonly called transition alumina [1]. Among transition alumina, γ polymorph is most frequently used since it possesses a large specific surface area, fair mechanical strength, thermal stability and the ability of active phase dispersion [2], which make it suitable for use in heterogeneous catalytic applications [3]. Therefore, γ -Al₂O₃ based catalysts are utilized in numerous chemical processes such as hydrodesulfurization, cracking, metathesis, etc. [4], as well as in three-way automotive catalysts [5, 6].

With the aim of preparing γ -Al₂O₃ possessing an increased specific surface area, various methods have been investigated, such as precipitation, hydrothermal, combustion, microwave synthesis etc. [7], one of them being sol–gel

synthesis. The sol–gel method is deemed to be an attractive chemical route for the preparation of metal oxide materials, finding its use in many different fields including catalysis [2]. The advantages of the sol–gel process, among others, are the achievement of a high surface area and optimal pore size distribution, as well as enhanced chemical reactivity of the oxide surface [8]. Hence, the sol–gel technique is broadly applied for alumina synthesis [4]. Most commonly used precursors for the sol–gel synthesis are metal alkoxides, but their drawbacks are high reaction rates which cause the formation of precipitates rather than gels. Their reactivity can be retarded by chelation, i.e. substitution of alkoxy groups by ligands forming a strong chemical bond with the metal. The reduction of the number of hydrolysable alkoxy groups results in a lowered hydrolysis rate [9].

In our previous publications, we report on chelate compounds obtained by chelation of aluminium sec-butoxide (Asb) with different amounts of ethyl acetoacetate (Eaa) [10], the features and morphology of the gels, as well as the texture of transition alumina which was attained by thermal treatment of the gels [11]. However, thermal stability of γ -alumina is of crucial importance for the catalytic application [12]. Also, thermal decomposition of the prepared chelates could be of interest due to the utilization of tris(ethyl

✉ S. Kurajica
stankok@fkit.hr

¹ Faculty of Chemical Engineering and Technology,
University of Zagreb, Marulićev trg 19, Zagreb, Croatia

² Pliva Croatia Ltd., Prilaz baruna Filipovića 25, Zagreb,
Croatia

acetoacetate)aluminium(III) as a precursor for MOCVD process [13, 14]. Therefore, this paper addresses the thermal evolution of gels obtained by chelation of Asb with Eaa and the influence of Eaa to Asb ratio on the thermal evolution of the prepared gels.

Experimental

Six gels were prepared, using aluminium sec-butoxide, Asb, $[\text{Al}(\text{OsBu})_3]$, 97%, Aldrich, Great Britain] and ethyl acetoacetate, Eaa, ($\text{C}_6\text{H}_{10}\text{O}_3$, 99%, Fluka, Germany), with Eaa/Asb molar ratios of 0.5, 1, 1.5, 2, 2.5 and 3, marked EA0.5, EA1.0, EA1.5, EA2.0, EA2.5 and EA3.0, respectively. Synthesis was carried out by adding 0.1 mol of Asb to the adequate amount of Eaa (0.05, 0.1, 0.15, 0.2, 0.25 and 0.3 mol) with a syringe to minimize air humidity subjection and the mixture was left stirring in a closed reactor for 24 h at room temperature with no sighted precipitation. The acquired clear sol was put into a large Petri dish, so as to enable maximal exposure to air moisture, and then held at room temperature until gelation occurred. The gel was left to dry for 5 days at room temperature causing the evaporation of the solvent and the release of alkoxy groups, which lead to a dry product. The resulting sample was ground to fine powder in a mortar and stored.

Scanning electron microscopy (SEM) performed on TESCAN VEGA3 was used for the investigation of surface morphology of the samples. Prior to analysis, samples were deposited on an adhesive surface and Au/Pd coated with Quorum SC 7620 coater.

Particle size distribution (PSD) was determined by the Low Angle Laser Light Scattering (LALLS) method on a Mastersizer 2000 Hydro S (Malvern Instruments) cell in the measuring range 0.01–1000 μm . The ISOPAR™ G— isoparaffin liquid (ExxonMobil) was used as the dispersant

with the addition of non-ionic surfactant SPAN®80 (Sigma-Aldrich). Every sample was analyzed 10 times for 5 s.

The thermal evolution of the prepared gels was established with differential thermal and thermo-gravimetric analysis (DTA/TGA) on Netzsch STA 409C thermo analyzer. Approximately 50 mg of the investigated material were placed in a Pt crucible and heated to 1300 °C at a heating rate of 10 °C min^{-1} in a synthetic air flow of 30 $\text{cm}^3 \text{min}^{-1}$ with α -alumina used as a reference.

IR spectra were obtained using the Fourier transform infrared spectrometer Bruker Vertex 70 in attenuated total reflectance (ATR) mode. Samples were pressed on a diamond, after which the absorbance data were collected between 400 and 1750 cm^{-1} with spectral resolution of 1 cm^{-1} and 64 scans.

Powder X-ray diffraction (XRD) was executed using Shimadzu diffractometer XRD 6000 with $\text{CuK}\alpha$ radiation working in a step scan mode with steps of 0.02° and counting time of 0.6 s Data were collected in a range between 5° and 70° 2θ .

Results and discussion

Morphology and gradation

Two distinct morphologies are noticeable in SEM micrographs of investigated samples, irregular chunks possessing a smooth surface (Fig. 1a) and agglomerated irregular particles (Fig. 1b). The former morphology is rarely observed in literature and resembles the amorphous synthesis products as reported by Mohamed et al. [15]. In our former investigation [11], we determined that the particles of the first type are gel units, while the second type particles are chelate, i.e. tris(ethyl acetoacetate)aluminium(III) agglomerates. The gel to chelate ratio depends on the Eaa/Asb ratio and with the

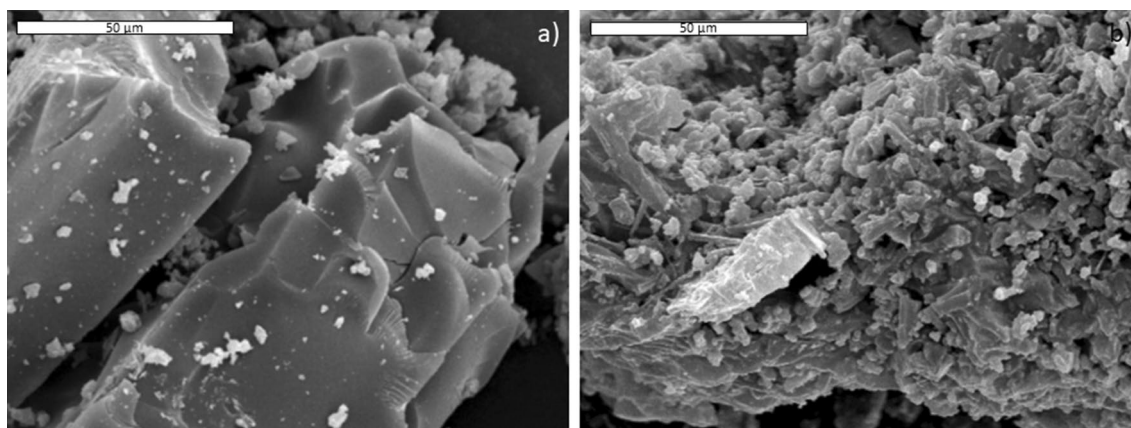


Fig. 1 SEM micrographs of samples **a** EA1.0 and **b** EA2.0

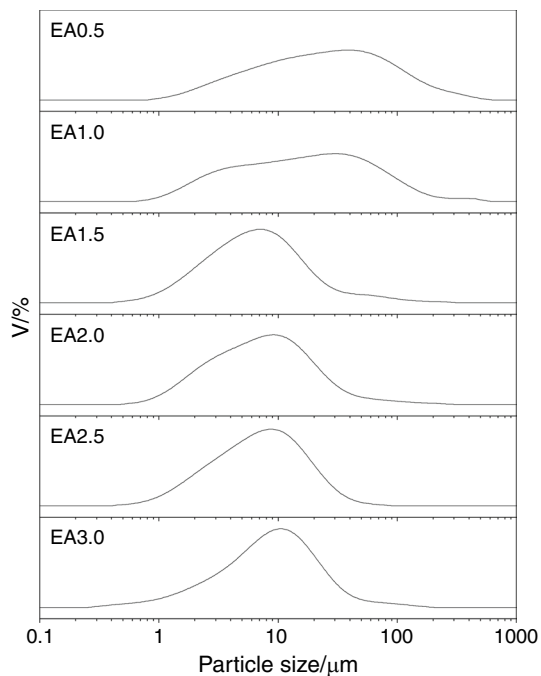


Fig. 2 Volume particle size distribution of the samples EA0.5–EA3.0 in the range of 0.01–1000 μm

Table 1 Particle size distribution of the samples EA0.5–EA3.0

Sample	D10/ μm	D50/ μm	D90/ μm
EA0.5	4.2	25.2	118
EA1.0	2.7	15.1	61.9
EA1.5	2.3	6.8	20.8
EA2.0	1.9	6.8	22.8
EA2.5	1.9	7.0	19.0
EA3.0	2.2	8.9	26.2

increase of this ratio the amount of the chelate increases as well [11]. The chelate is extremely resistant to hydrolysis and does not partake in the gelation process. Accordingly, gelation occurred in samples with a low Eaa/Asb ratio, but in samples with a high Eaa/Asb ratio polycondensation was almost insignificant.

Gel–chelate duality was further explored through laser diffraction particle size analysis. Figure 2 shows the particle size distribution curves of hydrolyzed samples EA0.5–EA3.0, while particle size distribution parameters are given in Table 1.

As can be observed in Fig. 2 and Table 1, particle size distributions of samples EA0.5 and EA1.0 are bimodal, while others can be assessed as monomodal with slightly noticeable asymmetry. The particle size distribution results are consistent with SEM observations pointing out to the existence of large gel and small chelate particles. An initial decrease of particle size with the increase of the Eaa/Asb ratio can be seen. Thus, D50 is approximately 25 μm for sample EA0.5, after which it decreases to $\sim 15 \mu\text{m}$ for sample EA1.0 and then to $\sim 7 \mu\text{m}$ for sample EA1.5. With further increase of the Eaa/Asb ratio, D50 does not change significantly. Based on the PSD, it is evident that substantial amounts of gel are present solely in samples EA0.5 and EA1.0, while the chelate dominates in the rest of the samples. In their study of sol–gel derived amorphous alumina powders Schinkel et al. [16] established particles median size in the range between 6 and 12 μm , which is closer to our samples with higher Eaa/Asb ratio.

Thermal analysis

Thermal properties of the prepared samples were evaluated by differential thermal and thermo-gravimetric analysis.

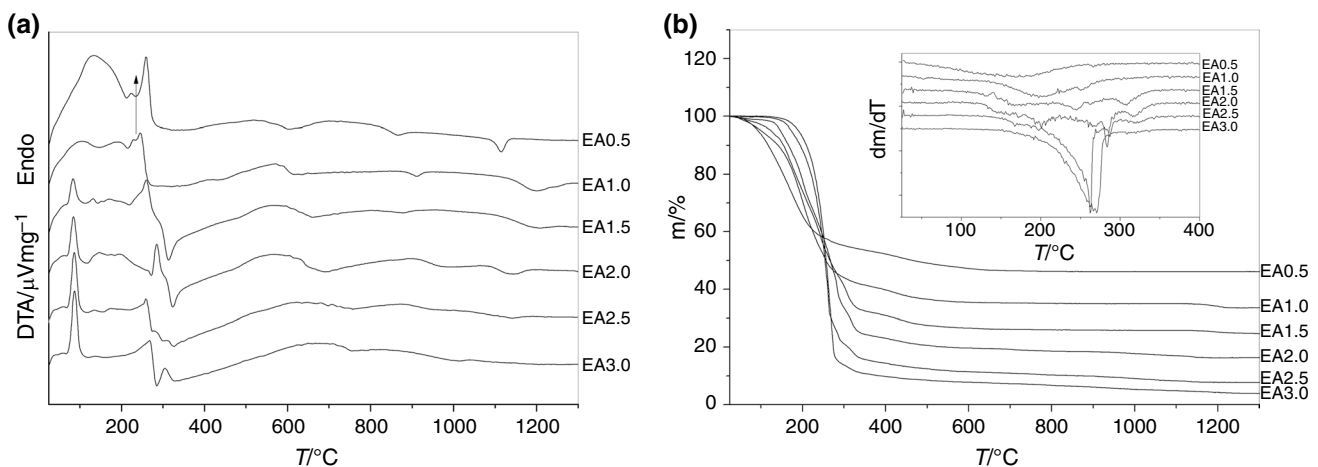


Fig. 3 **a** DTA and **b** TGA curves of the samples EA0.5–EA3.0 obtained with a heating rate of $10 \text{ }^\circ\text{C min}^{-1}$ in dynamic air. Inset: DTG curves of the samples EA0.5–EA3.0. DTA and DTG curves are shifted for visualization purposes

DTA curves (Fig. 3a) exhibit a sharp endothermic peak centered at ~ 88 °C and an endothermic peak between 100 and 140 °C, which are both superimposed on a broad endothermic peak in a range between room temperature and 200 °C. Similar succession of endothermal and exothermal peaks was noted in a study of tris(acetylacetonate)aluminum(III) decomposition [17]. Another endothermic peak appears in a range between 200 and 300 °C. Exothermic peaks can be observed in the following ranges: 300–350 °C (except for samples EA0.5 and EA1.0), 600–750 °C, 850–1000 °C and 1100–1200 °C (except for sample EA3.0).

The mass loss of the samples is conspicuous in the entire temperature range, from room temperature to 1300 °C. Based on the DTG curves (Fig. 3b inset), four mass loss intervals could be distinguished: slow mass loss process in the interval between room temperature and 300 °C centered at ~ 200 °C, rapid mass loss between 200 and 300 °C concentrated at 260–280 °C, small and rapid mass loss around 285 °C discernible only for samples EA2.0 and EA2.5, and finally small and slow mass loss around 315 °C visible only in samples EA1.5, EA2.0 and EA2.5. Two additional mass loss intervals could be observed from the TGA curves in intervals 350–700 °C and 700–1300 °C. Rapid mass loss in the approximately same temperature interval for tris(acetylacetonate)aluminum(III) decomposition is reported by Lalancalette [17]. Similar decomposition temperatures are reported for other metal chelates, e.g. copper acetylacetonate [18].

Structural analysis of samples quenched from various temperatures

In order to ascribe peaks to specific processes, the heating of all samples was disrupted at several temperatures between 200 and 1200 °C. The collected samples were then examined using FTIR spectroscopy and XRD analysis, and the obtained results are presented in Figs. 4 and 5.

FTIR spectra of samples EA0.5 to EA3.0 are shown in Fig. 4. The majority of spectra of the as prepared samples, which were not subjected to thermal treatment, possess characteristic absorption bands at ~ 1610 cm^{-1} due to C=O stretching vibrations of ethyl acetoacetate linked to aluminium in the chelate [19–23], as well as an absorption band of C–C vibrations in the six membered ring of the chelate complex at 1520 cm^{-1} [23, 24]. All other detected bands due to Eaa–Al chelate are: bands of C–C stretching, –C–C–O stretching and O–C–C stretching at ~ 1290 , ~ 1170 and ~ 1060 cm^{-1} , respectively [20, 21, 23, 25], and bands at ~ 620 and ~ 510 cm^{-1} attributed to ring deformation modes [26]. Bands characteristic for esters, because of methylene twisting and wagging vibrations, appear at ~ 1310 and 1020 [25]. Bands which are the result of the presence of methyl groups (at ~ 2980 cm^{-1} , ~ 2870 cm^{-1} , ~ 1480 cm^{-1} , ~ 1420

cm^{-1} and ~ 1370 cm^{-1}) and methylene groups (at ~ 2930 and ~ 2840 cm^{-1}) are also present [21–23, 25]. The signals observed at ~ 990 and ~ 740 cm^{-1} are assigned to the stretching mode of Al–O vibrations [27, 28], while signals noted at ~ 450 and ~ 420 are ascribed to the bending modes of Al–O vibration [27, 28]. In the majority of the spectra, a weak broad band between 3800 and 2800 cm^{-1} corresponding to O–H stretching vibrations can be seen [29]. The hydroxyl groups' vibrations are usually a consequence of the presence of adsorbed water, but also result from hydroxyl groups bonded to aluminium [30] due to hydrolysis in the course of the gelation process.

Chelate bands in spectra of as-prepared samples are imperceptible for samples EA0.5 and EA1.0 and show increased intensity from sample EA0.5 to sample EA3, which is an obvious consequence of the increase of the Eaa/Asb ratio in the samples. The spectra of the as-prepared samples also show a broad band in the range from 800 to 400 cm^{-1} . The intensity of this band is considerable for samples EA0.5 and EA1.0, while it diminishes with the increase of the Eaa/Asb ratio in the samples. This band stems from the Al–O–Al bonds formed by condensation during the gelation process [31]. Obviously, the extent of the hydrolysis process is dependent on the Eaa/Asb ratio, and while the gelation process is advanced for samples Ea0.5 and EA1.0, it gets weaker with more Eaa in the samples. According to the intensity of this band, it could be concluded that almost no hydrolysis and condensation occur in the sample EA3.0. In other words, it is clear that Eaa efficiently retarded the hydrolysis and condensation processes, and the greater the Eaa/Asb ratio is, the slower will be the hydrolysis. Knowing that there are practically no butoxide groups present [11], since only tris(ethyl acetoacetate)aluminium(III) chelate molecules were detected in the gel samples via ^1H NMR spectroscopy [11], the samples could be described as comprised of partially condensed alumina network and tris(ethyl acetoacetate)aluminium(III), where the amount of the gel and the chelate depends on the original Eaa to Asb ratio. Thus, samples with a low Eaa to Asb ratio are predominantly amorphous and cross-linked through oxo-bridges, while samples with a great Eaa to Asb ratio are chiefly chelate.

FTIR spectra of samples thermally treated at 200 °C are quite similar to the spectra of samples which were not thermally treated; the only difference being the bands' intensity. On the other hand, in the FTIR spectra of samples thermally treated at 400 °C, chelate bands disappear entirely. The spectra of samples quenched from temperatures between 400 and 1000 °C are characterized by a single broad band in the range from 800 to 400 cm^{-1} due to Al–O–Al bonds. For samples thermally treated at 1200 °C, only bands at ~ 640 , ~ 570 , ~ 490 and ~ 420 cm^{-1} , assigned to the stretching and bending modes of Al–O vibrations, which are typical for α -alumina [28, 29, 32], could be observed (Fig. 4).

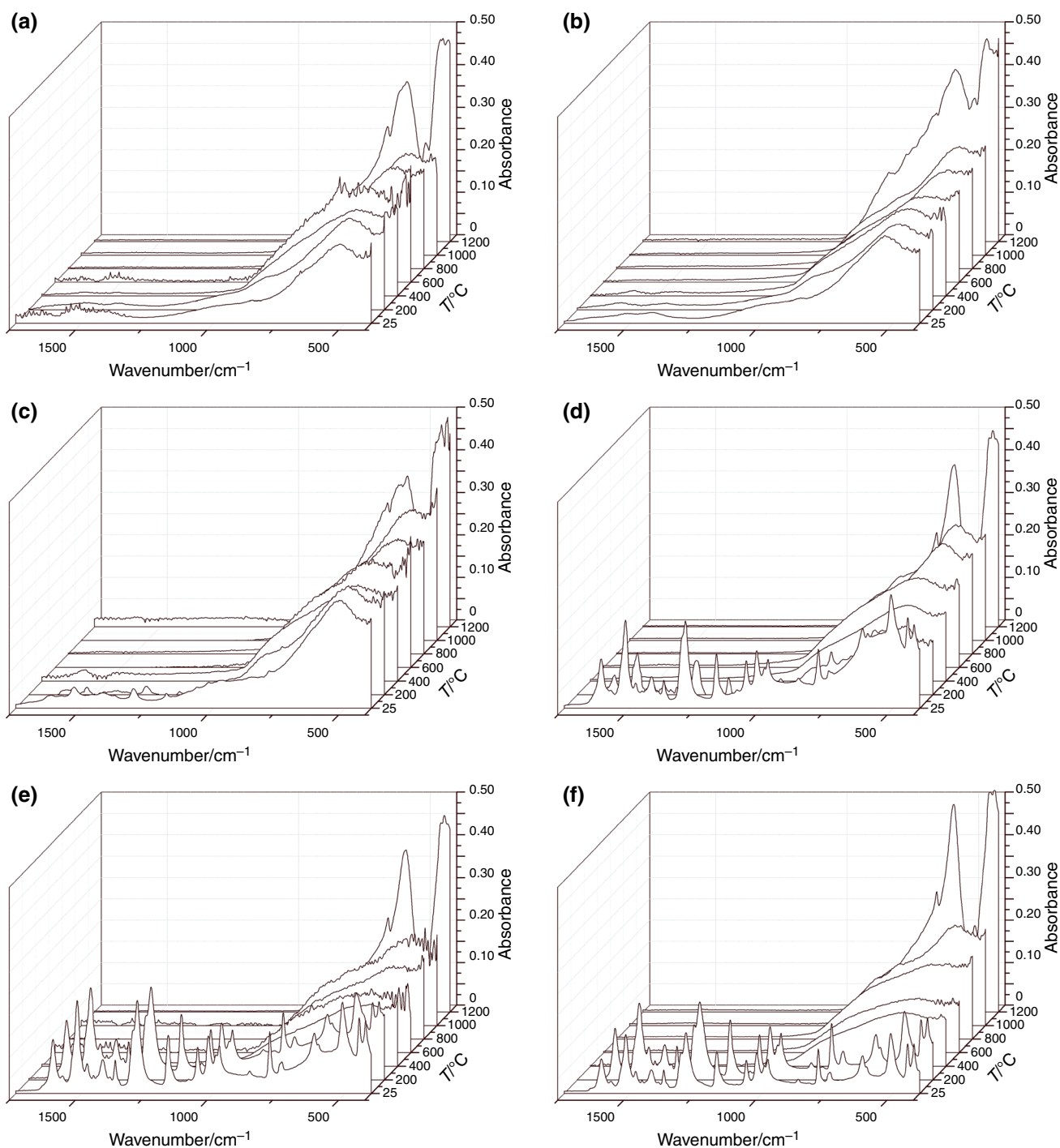


Fig. 4 FTIR spectra of samples **a** EA0.5, **b** EA1.0, **c** EA1.5, **d** EA2.0, **e** EA2.5 and EA3.0 quenched from various temperatures specified in the figure in wavelength interval between 1500 and 400 cm^{-1} , as-prepared sample is marked with 25 $^{\circ}\text{C}$

XRD patterns of as-prepared samples EA0.5 and EA1.0 (Fig. 5a and b) are mostly typical patterns of amorphous gels, showing only few broad humps. However, few faint peaks consistent with tris(ethyl acetoacetate)aluminium(III) [33] can be identified. Peaks belonging to tris(ethyl acetoacetate)aluminium(III), also superimposed on amorphous

humps, are far better perceptible in patterns of the as-prepared samples EA1.5, EA2.0, EA2.5 and EA3.0 (Fig. 5c–f). The intensity of tris(ethyl acetoacetate)aluminium(III) peaks increases from sample EA0.5, where only few vague peaks could be observed, to sample EA3.0, which exhibits a pattern typical for a well crystallized phase.

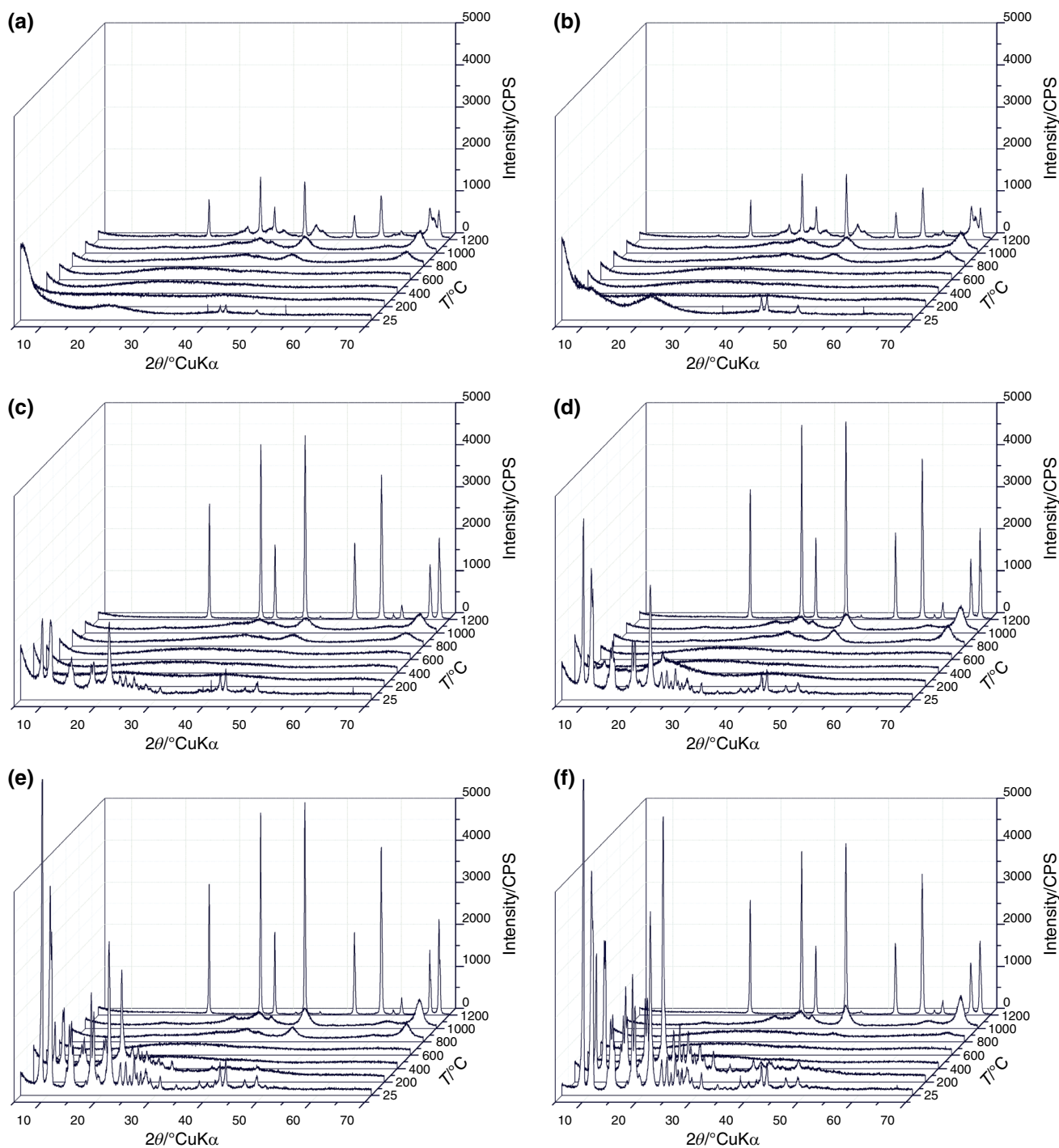


Fig. 5 Powder XRD patterns of samples **a** EA0.5, **b** EA1.0, **c** EA1.5, **d** EA2.0, **e** EA2.5 and **f** EA3.0 quenched from various temperatures specified in the figure. As-prepared sample is marked with 25 °C

XRD patterns of samples quenched from 200 °C are similar to room temperature patterns, but with diminishing tris(ethyl acetoacetate)aluminium(III) peaks. Samples treated at 400 and 600 °C are completely amorphous. The patterns of the samples treated at 800 °C contain broad peaks corresponding to γ -Al₂O₃ (ICDD PDF No. 10-0425).

Peaks of γ -Al₂O₃ grow stronger in the patterns of the samples treated at 1000 °C, while the patterns of the samples treated at 1200 °C reveal a transformation to α -Al₂O₃ (ICDD PDF No. 10-0173). Transformation is complete for samples EA1.5 to EA3.0, which is manifested in the appearance of sharp α -Al₂O₃ peaks only, while for samples EA0.5

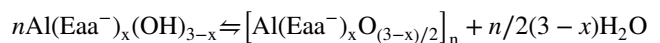
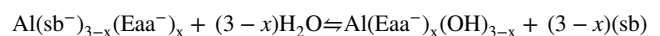
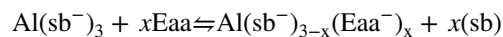
and EA1.0 quenched from 1200 °C several residual broad γ -Al₂O₃ peaks could be observed indicating that the transformation of γ -Al₂O₃ to α -Al₂O₃ is only partial (Fig. 5).

Thermal evolution of gels

Therefore, on the basis of FTIR and XRD analysis, thermal events detectable on DTA and TGA curves can be assigned as follows: Broad endothermic peak in the range between room temperature and 200 °C, accompanied by a mass loss, can be ascribed to the evaporation of water and possibly free Eaa [21]. Sharp endothermic peak centered at ~88 °C without mass loss is a consequence of polymorphic transition of tris(ethyl acetoacetate)aluminium(III). Subsequent endothermic and exothermic peaks in the temperature range between 200 and 350 °C accompanied by mass loss can be attributed to the further decomposition of the chelate and burning of organic groups [21, 34], as well as the loss of structural water if present (through additional gel condensation). [35, 36] Lalancette et al. [17] report on a rapid mass loss between 160 and 240 °C due to the aluminum tris(acetylacetonate)aluminum(III) decomposition, which points to a slightly greater thermal stability of tris(ethylacetoacetate)aluminum(III). It could be postulated that throughout the decomposition and burning of the organics, a certain amount of amorphous carbon accumulates due to incomplete oxidation. Exothermic peaks between 600 and 750 °C and between 850 and 1000 °C are both due to the crystallization of γ -alumina. The SEM, FTIR and XRD measurements all demonstrate that there are two γ -alumina precursors in the samples, the chelate and the gel. At these temperatures, the chelate and/or the gel no longer exist, but their decomposition products could differ in microstructure and purity. However, it is not easy to attribute a certain peak to a specific crystallization process. First of all, both peaks appear on all six DTA curves. The peak due to the crystallization of the chelate decomposition products should be greater with the greater Eaa/Asb ratio. On the other hand, the peaks should diminish in intensity with the increase of the Eaa/Asb ratio. The reason for that is a larger mass loss prior to crystallization because of chelate decomposition in the samples with greater Eaa/Asb ratio. On account of greater mass loss, the amount of crystallized Al₂O₃ decreases, less energy is released and the peak is smaller. As a result, no clear trend in the first peak intensity could be discovered. The second peak shows somewhat greater intensity on the curves of samples EA0.5 and EA1.0. Since those samples are rich in gel and almost completely without the chelate, based on the higher intensity of the second peak, it may be concluded that the second peak is the consequence of the crystallization of γ -alumina from the gel, while the first one is the result of crystallization of γ -alumina from the

chelate. The last exothermic peak is the outcome of the transformation of γ - to α -alumina. This peak also declines in intensity with the increase of the Eaa/Asb ratio due to a greater mass loss prior to crystallization. Alipour et al. report on a similar gel crystallization sequence at ~900 and 1100 °C [37]. Therefore, gel/chelate duality, besides on the structure and microstructure, reflects on the thermal evolution, i.e. thermal analysis curves (Fig. 3a and b) of the samples yielding with differences in the peaks appearance and intensity, dependent on the Eaa/Asb ratio, i.e. various amounts of the gel and chelate.

The TGA results show that the magnitude of the mass loss increases with the increase of the Eaa/Asb ratio, i.e. with the increase of the organic content. The total mass losses of the samples according to the TG analysis, in comparison with theoretical mass losses, are given in Table 2. The theoretical mass loss was calculated based on the assumption that the overall content of the gel samples could be represented with a simplified formula Al(Eaa)_xO_{(3-x)/2}, where x is the Eaa to Asb ratio. This assumption implies a complete chelation of the Asb, so that none of the Eaa, but all of the alkoxy groups were expelled from the sample during hydrolysis, condensation and drying processes. In other words, it was presumed that the chelation, hydrolysis and condensation processes could be represented by chemical equations:

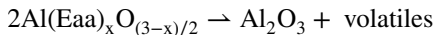


where sb⁻ denotes the sec-butoxy group (O⁻Bu⁻), sb symbolizes the sec-butanole (BuOH), Eaa⁻ signifies the enolate of ethyl acetoacetate (C₆H₉O₃⁻), Eaa means ethyl acetoacetate (C₆H₁₀O₃), x is the Eaa to Asb ratio and n is any integer equal or greater than two.

Table 2 Theoretical and actual mass loss of investigated samples

Sample	Theoretical mass loss/%	Actual mass loss/%
EA0.5	0.54	0.54
EA1.0	0.70	0.67
EA1.5	0.78	0.75
EA2.0	0.83	0.84
EA2.5	0.86	0.92
EA3.0	0.88	0.96

Under this premise, the overall process occurring in the course of thermal analysis could be represented with the reaction:



As can be seen in Table 2, the mass losses of samples EA0.5 to EA2.0 are close or slightly smaller than theoretical, whilst for the samples EA2.5 and EA3.0 they are greater than theoretical. Losses which are smaller than theoretical are the result of partial hydrolysis of a small share of Eaa. Hence, some amount of Eaa has been removed from the chelate and evaporated prior to thermal analysis and in those cases x is in fact smaller than the initial Eaa/Asb ratio. Mass losses that are greater than theoretical can be explained with vaporization of tris(ethyl acetoacetate)aluminium(III), since it boils in the temperature range between 190 and 200 °C [38]. For this reason, it is not a surprise that in samples rich in tris(ethyl acetoacetate)aluminium(III), its small amount vaporizes in the course of the analysis.

Conclusions

The thermal evolution of gels prepared by chelation of aluminum sec-butoxide with ethyl acetoacetate in various amounts was investigated. Samples with a low Eaa to Asb ratio are primarily amorphous and cross-linked through oxo-bridges, while samples with a great Eaa to Asb ratio mostly consist of the chelate. In such manner, thermal evolution is influenced by the Eaa to Asb ratio showing a greater mass loss with a greater Eaa to Asb ratio. Samples mass loss is in concordance with the conjecture that the overall content of the gel samples could be represented with a simplified formula $\text{Al}(\text{Eaa})_x\text{O}_{(3-x)/2}$, where x is the Eaa to Asb ratio. For all samples, the crystallization of $\gamma\text{-Al}_2\text{O}_3$ occurs in the form of two processes between 600 and 1000 °C. The transition of $\gamma\text{-Al}_2\text{O}_3$ to $\alpha\text{-Al}_2\text{O}_3$ for samples with a high Eaa to Asb ratio is complete at 1200 °C, while the same transition is only partial for samples having a low Eaa to Asb ratio. Beside thermal evolution, gel-chelate duality of the samples reflects on the morphology and particle size distribution.

Acknowledgements This work has been supported by the projects IP-2018-01-2963 HOUDINI and UIP-2019-02-2367 SLIPPERY SLOPE of the Croatian Science Foundation, bilateral project “NMR characterization of aluminium sec-butoxide modified with ethyl acetoacetate at different ratios” of the Ministry of Science, Education and Sport of the Republic of Croatia and Ministry of Education, Science and Sport of the Republic of Slovenia, and PZS-2019-02-1555 PW-WALL in Research Cooperability Program of the Croatian Science Foundation funded by the European Union from the European Social Fund under the Operational Programme Efficient Human Resources 2014–2020. The aegis of the University of Zagreb is gratefully acknowledged.

Author contributions SK: conceptualization, SK, KM, IS, VM: methodology, SK, KM, IS, VM: formal analysis and investigation, SK: writing—original draft preparation, SK, KM, IS, VM: writing—review and editing, SK, KM, VM: visualization, SK: supervision, SK and VM: project administration, SK and VM: funding acquisition. All authors have read and agreed to the published version of the manuscript.

Data availability The data and material are available upon request.

Code availability Not applicable.

Declarations

Conflict of interest No conflict of interest.

References

1. Stuart NM, Sohlborg K. The microstructure of γ -alumina. *Energies*. 2021;14:6472.
2. Akia M, Mahdi Alavi S, Rezaei M, Yan Z-F. Optimizing the sol-gel parameters on the synthesis of mesostructured nanocrystalline $\gamma\text{-Al}_2\text{O}_3$. *Microporous Mesoporous Mater*. 2009;122:72–8.
3. Busca G. The surface of transitional aluminas: a critical review. *Catal Today*. 2014;226:2–13.
4. Aguado J, Escola JM, Castro MC, Paredes B. Sol-gel synthesis of mesostructured γ -alumina templated by cationic surfactants. *Microporous Mesoporous Mater*. 2005;83:181–92.
5. Wang J, Chen H, Hu Z, Yao M, Li Y. A review on the Pd-based three-way catalyst. *Catal Rev*. 2015;57:79–144.
6. Jing Y, Wang G, Ting KW, Maeno Z, Oshima K, Satokawa S, Nagoka S, Shimizu K-I, Toyao T. Roles of the basic metals La, Ba, and Sr as additives in Al_2O_3 -supported Pd-based three-way catalysts. *J Catal*. 2021;400:387–96.
7. Frikha K, Limousy L, Bouaziz J, Bennici S, Chaari K, Jegurim M. Elaboration of alumina-based materials by solution combustion synthesis: a review. *Comptes Rendus Chim*. 2019;22:206–19.
8. Crisan M, Zaharescu M, Kumari VD, Subrahmanyam M, Crisan D, Dragan N, Raileanu M, Jitianu M, Rusu A, Sadanandam G, Reddy JK. Sol-gel based alumina powders with catalytic applications. *Appl Surf Sci*. 2011;258:448–55.
9. Lichtenberger R, Puchberger M, Baumann SO, Schubert U. Modification of aluminum alkoxides with *b*-ketoesters: new insights into formation, structure and stability. *J Sol-Gel Sci Technol*. 2009;50:130–40.
10. Kurajica S, Gazivoda Kraljević T, Mali G, Simčić I, Mandić V, Minga I. Multinuclear magnetic resonance study on aluminium sec-butoxide chelated with ethyl acetoacetate in various amounts. *Croat Chem Acta*. 2019;92:17–28.
11. Kurajica S, Mali G, Mandić V, Simčić I, Matijašić G, Mužina K. Tailoring microstructural, textural and thermal properties of transition-alumina by modifying aluminum sec-butoxide with ethyl acetoacetate within a sol-gel synthesis. *J Phys Chem Solids*. 2021;148:109783.
12. Rossignol S, Kappenstein C. Effect of a doping elements on the thermal stability of transition alumina. *Int J Inorg Mater*. 2021;3:51–8.
13. Ito A, Tu R, Goto T. Amorphous-like nanocrystalline $\gamma\text{-Al}_2\text{O}_3$ films prepared by MOCVD. *Surf Coat Technol*. 2010;204:2170–4.
14. Grimm S, Baik S-J, Hemberger P, Bodi A, Kempf AM, Kasper T, Atakan B. Gas-phase aluminium acetylacetonate decomposition: revision of the current mechanism by VUV synchrotron radiation. *Phys Chem Chem Phys*. 2021;23:15059–75.

15. Mohamed RM, Ismail AA, Kini G, Ibrahim IA, Koopman B. Synthesis of highly ordered cubic zeolite A and its ion-exchange behavior. *Colloids Surf A*. 2009;348:87–97.
16. Schinkel G, Garn I, Frank B, Gernert U, Schubert H, Schomacker R. Fabrication of alumina ceramics from powders made by sol-gel ty hydrolysis in microemulsions. *Mat Chem Phys*. 2008;111:570–7.
17. Lalancalette RA, Sydek F, Grebowicz J, Arslan E, Bernal I. The thermal decomposition and analysis of metal trys-acetylacetonates. *J Therm Anal Calorim*. 2019;135:3463–70.
18. Wiecinski P, Wieclaw-Midor A. Metal salts as dopants for ZnO ceramics—thermogravimetry coupled with mass spectrometry studies. *J Therm Anal Calorim*. 2021. <https://doi.org/10.1007/S10973-021-10934-9>.
19. Tadanaga K, Iwami T, Tohge N, Minami T. Precursor structure and hydrolysis-gelation process of Al(O-sec-Bu)₃ modified with ethylacetoacetate. *J Sol-Gel Sci Technol*. 1994;3:5–10.
20. Khelifi L, Ghorbel A. New gelation process for Pt/Al₂O₃ catalysts preparation. *J Sol-Gel Sci Technol*. 2003;26:847–52.
21. Jing C, Zhao X, Zhang Y. Sol-gel fabrication of compact, crack-free alumina film. *Mater Res Bull*. 2007;42:600–8.
22. Hoebbel D, Reinert T, Schmidt H. On the hydrolytic stability of organic ligands in Al-, Ti- and Zr-alkoxide complexes. *J Sol-Gel Sci Technol*. 1997;10:115–26.
23. Kurajica S, Mali G, Gazivoda T, Sipusic J, Mandic V. A spectroscopic study of calcium aluminate gels obtained from aluminium sec-butoxide chelated with ethyl acetoacetate in various ratios. *J Sol-Gel Sci Technol*. 2009;50:58–68.
24. Yamada N, Yoshinaga I, Katayama S. Formation behavior and optical properties of transparent inorganic-organic hybrids prepared from metal alkoxides and polydimethylsiloxane. *J Sol-Gel Sci Technol*. 2000;17:123–30.
25. Silverstein RM, Webster FX. *Spectrometric identification of organic compounds*. 6th ed. New York: Wiley; 1998.
26. Tayyari SF, Milani-Nejad F. Vibrational assignment of acetylacetonate. *Spectrochim Acta A*. 2000;56:2679–91.
27. Hoebbel D, Bhattacharya IN, Das SC, Mukherjee PS, Paul S, Mitra PK. Thermal decomposition of precipitated fine aluminium trihydroxide. *Scand J Metall*. 2004;33:211–9.
28. Shirodker M, Borker V, Nather C, Bensch W, Rane KS. Synthesis and structure of tris(acetylacetonato) aluminium(III). *Indian J Chem*. 2010;49:1607–11.
29. Velasco MJ, Rubio F, Rubio J, Oteo JL. DSC and FT-IR analysis of the drying process of titanium alkoxide derived precipitates. *Thermochim Acta*. 1999;326:91–7.
30. Nass R, Schmidt H. Synthesis of an alumina coating from chelated aluminium alkoxides. *J Non-Cryst Solids*. 1990;121:329–33.
31. Bonhomme-Courry L, Babonneau F, Livage J. Investigation of the sol-gel chemistry of ethylacetoacetate modified aluminum sec-butoxide. *J Sol-Gel Sci Technol*. 1994;3:157–68.
32. Hajduchova Z, Pach L, Lokaj J. Adsorption of dodecylbenzenesulfonic acid on the alumina particles in the preparation of alumina foam. *Ceram-Silik*. 2018;62:138–45.
33. Kurajica S, Popović J, Gazivoda Kraljević T, Tkalčec E, Simčić I, Mandić V, Altomare A, Moliterni A. Rocquefelte X A structural investigation of tris(ethyl acetoacetate) aluminium (III). *J Sol-gel Sci Technol*. 2014;71:217–23.
34. Gonzalez-Pena V, Marquez-Alvarez C, Diaz I, Grande M, Blasco T, Perez-Pariente J. Sol-gel synthesis of mesostructured aluminas from chemically modified aluminum sec-butoxide using non-ionic surfactant templating. *Microporous Mesoporous Mater*. 2005;80:173–82.
35. Chandradass J, Balasubramanian M. Sol-gel processing of alumina fibres. *J Mater Process Technol*. 2006;173:275–80.
36. Kim S-M, Lee Y-J, Jun K-W, Park J-Y, Potdar HS. Synthesis of thermo-stable high surface area alumina powder from sol-gel derived boehmite. *Mater Chem Phys*. 2007;104:56–61.
37. Alipour A, Jazayeri H, Nemati A, Mohammadpour AM. Preparation of submicron alumina from aluminum 2-methoxyethoxide. *Mater Lett*. 2001;48:15–20.
38. Charles GR, Paterson NC, Franke GH. Aluminium derivative of ethyl acetoacetate. In: Ann R, editor. *Inorganic synthesis Vol IX* Ed. Tyree SY. New York: McGraw-Hill Inc.; 1967. p. 25–7.

Publisher's Note Springer Nature remains neutral with regard to jurisdictional claims in published maps and institutional affiliations.